Journal of The Electrochemical Society, **155** (5) F82-F90 (2008)
0013-4651/2008/155(5)/F82/9/$23.00 © The Electrochemical Society

Poly(Vinyl Ferrocene) Redox Behavior in Ionic Liquids

Yijun Tang* **and Xiangqun Zeng****,z

Department of Chemistry, Oakland University, Rochester, Michigan 48309, USA

We describe in this report a systematic electrochemical characterization of the ion-solvent coupling mechanisms of poly(vinyl ferrocene) (PVF) in pure ionic liquid (IL) and 0.1 M IL aqueous solutions. Our study showed that the unique solvation and ionic properties of ILs significantly affected the break-in process and the ion-solvent transport mechanisms of PVF redox switching. A square model that emphasized both faradaic and nonfaradaic processes of PVF was used to explain the unique irreversible break-in effect in the pure ILs. The electrochemical quartz crystal microbalance technique was used to characterize the PVF redox processes in 0.1 M 1-butyl-3-methyl imidazolium tetrafluoroborate and 0.1 M methanesulfonate ILs in which an obvious difference of cyclic voltammogram was observed. Our results suggested the existence of strong IL-polymer interaction in 0.1 M methanesulfonate IL solutions, i.e., not only the anions but also the IL molecules interacted with the PVF matrix. The cations were later removed from the PVF matrix to balance the excessive positive charge in PVF oxidation. Our study confirmed that IL was not only an electrolyte but also a solvent in PVF redox switching processes. Various types of interactions between PVF and the IL, including dispersion, dipole induction, dipole orientation, hydrogen-bonding, or ionic/charge-charge interactions, could significantly change the PVF redox dynamics. Thus, IL tremendous diversity in structural and chemical properties and their distinctive properties offer us an excellent opportunity to explore IL-polymer interactions and to dynamically control the conductive polymer relaxation processes and their redox switching mechanism for various applications.
 [DOI: 10.1149/1.2868797]

Manuscript submitted November 23, 2007; revised manuscript received January 4, 2008. Available electronically March 11, 2008.

Electrodes modified with conductive polymers have been studied extensively for both practical and fundamental applications.[1] Electrochemical investigations showed that the transports of solvent, ion species within the conductive polymer films had a great impact not only on kinetics and thermodynamics of the redox behavior but also on the film surface structure.[2] The actual polymer structure that affected its electrochemical behavior strongly depended on the nature of the solvent and the supporting electrolyte as well as on the temperature. Extensive investigations of conductive polymer redox mechanisms were characterized either in aqueous electrolytes with various inorganic salts or in organic solvents such as acetonitrile with tetraalkylammonium salts.[3] Our motivation in this work is to study conductive polymer redox mechanisms in nonaqueous electrolyte, i.e., ionic liquids (ILs), and compare them with the typical aqueous electrolyte solutions. Being composed entirely of ions, ILs have a high intrinsic conductivity and show clear advantages over conventional solvents in which the use of supporting electrolytes is required for electrochemistry study. ILs possess high ion concentration, high heat capacity, and good electrochemical stability. They prove to be excellent electrolytes for electrochemical devices including super capacitors, fuel cells, lithium batteries, photovoltaic cells, electrochemical mechanical actuators, and electroplating, as well as excellent candidates for highly efficient heat-transfer fluids and supporting media for catalysts.[4] Therefore, studying the redox mechanisms of conductive polymers in IL is significant for both fundamental and applied researches. Poly(vinyl ferrocene) (PVF) was selected as our conductive polymer system because it is one of the most studied polymers by electrochemical techniques. The behavior of the ferrocene/ferrocenium couple has already been well characterized, and the redox process of the monomer is a simple, reversible, one-electron transfer, so we are able to compare our results with those well characterized in the literature.

Pickup and Osteryoung were the first to investigate PVF redox switching in an IL (also called molten salt) containing aluminum chloride and butylpyridinium chloride.[5] These types of ILs are less stable and are sensitive to water.[6] In the last decade, a series of ILs based on the cations of alkylpyridinium or dialkylimidazolium were developed. The anions varied from halides, such as Cl^-, Br^-, or $AlCl_4^-$, to coordinates, such as BF_4^-, PF_6^-, SbF_6^-, or NO_3^-, SO_4^-, $CuCl_2^-$, and organics, such as $CH_3SO_3^-$ or $(CF_3SO_2)_2N^-$.[7] ILs are classified into three basic classes: aprotic, protic, and zwitterionic. Aprotic ILs such as the alkyl imidazolium-based ILs comprising an imidazolium cation and an organic anion of BF_4^- or PF_6^- are more water- and air-stable.[6] They show excellent mechanical strength, chemical stability, and ionic conductivity. As a result, we describe here our study of the PVF redox switching in aprotic ILs by systematic electrochemical characterization of the ion-solvent coupling mechanisms of PVF in pure ILs, aqueous IL solutions, and 0.1 M $NaClO_4$.

One of the well-known phenomena in the conductive polymer research is the break-in effect, i.e., the first cycle is different from the following cycles in cyclic voltammograms (CVs). The microscopic origin of these relaxation and hysteresis phenomena were interpreted in terms of slow morphological changes and/or the difficulty of removing remaining charges from insulating surroundings,[8] but it was never well-understood. We hypothesize that various types of interactions between conductive polymer and the IL such as dispersion, dipole induction, dipole orientation, hydrogen bonding, or ionic/charge–charge interactions could significantly affect the conductive polymer relaxation processes. Consequently, we studied the role of the dynamical IL-polymer interactions on the PVF electrochemical properties in order to relate these properties of the conductive polymers with their microscopic structural changes. We selected all water-soluble ILs for the following two reasons. First, water-soluble ILs allow us to further study the PVF redox mechanism in the IL solutions so that we can correlate both systems. Second, water-soluble ILs possess high polarities, which may also possess high conductivities. Our study showed that IL-polymer interactions at open-circuit conditions could eliminate the break-in effect. Further electrochemical quartz crystal microbalance (EQCM) studies in IL solutions revealed that the interaction between IL and PVF was largely determined by the anion of the IL. A multistep doping/undoping mechanism was proposed for the PVF redox processes in the aqueous solutions of methanesulfonate ILs.

Experimental

Materials.— PVF (MW ~50,000, cat # 09746) was purchased from Polysciences, Inc., tetrabutylammonium perchlorate (TBAP, cat # 394) was purchased from GFS Chemicals, dichloromethane (CH_2Cl_2, cat # 61005-0040) was purchased from Acros Organics, sodium methanesulfonate (NaOMs, cat # 304506) was purchased from Aldrich, and sodium perchlorate ($NaClO_4$, cat # S1513) was purchased from Sigma. We tested seven methanesulfonate ILs and three 1-butyl-3-methyl imidazolium ILs: tetrabutylphosphonium methanesulfonate ([Bu_4P][OMs]), tetrabutylammonium methanesulfonate ([Bu_4N][OMs]), 1-butyl-3-ethyl imidazolium methanesulfonate ([BEIM][OMs]), 3-methyl-1-propyl imidazolium

* Electrochemical Society Student Member.
** Electrochemical Society Active Member.
z E-mail: zeng@oakland.edu

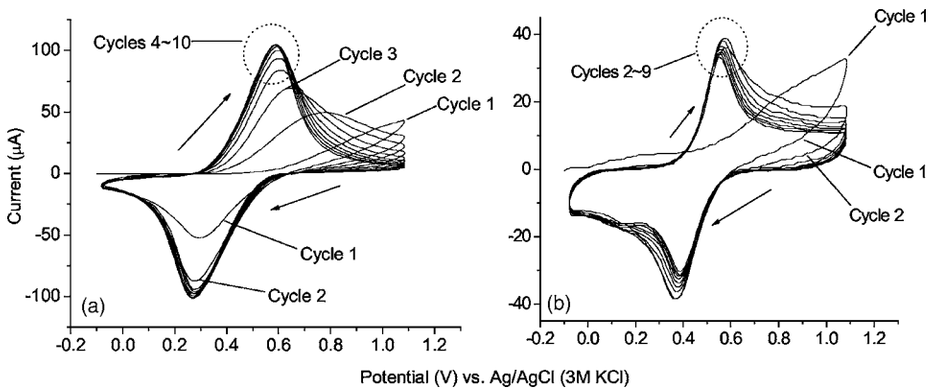

Figure 1. Break-in effect as observed (a) in pure [BMIM][BF_4] and (b) in pure [PMIM][OMs]. Potential scan rate was 200 mV/s. All experiments were done in freshly made PVF films that had been characterized in 0.1 M $NaClO_4$ only.

methanesulfonate ([PMIM][OMs]), 1-butyl-2-methyl-3-methyl imidazolium methanesulfonate ([BMMIM][OMs]), 1-ethyl-3-methyl imidazolium methanesulfonate ([EMIM][OMs]), 1-butyl-3-methyl imidazolium methanesulfonate ([BMIM][OMs]), 1-butyl-3-methyl imidazolium tetrafluoroborate ([BMIM][BF_4]), and 1-butyl-3-methyl imidazolium hydrogen sulfate ([BMIM][HSO_4]). [BMIM][BF_4] (cat # 29164) and [EMIM][OMs] (cat # 91508) were purchased from Sigma. All the other ILs were a gift from Dr. Rex Ren of IL-TECH Inc. (Middletown, CT) with purities over 98%. The 10 MHz quartz crystal with gold plate electrodes were purchased from the International Crystal Manufacturing Company, Inc. (Oklahoma City).

PVF film.— PVF film was electrochemically deposited onto the gold plate electrodes of a 10 MHz AT-cut quartz crystal in dichloromethane as described by Bruckenstein.[9] In brief, the dichloromethane solution contained 0.1 M TBAP and 2.5 mM PVF. Potential was applied to the gold electrode at 0.7 V for 3 min and 0 V for another 3 min. This cycle was conducted three times in total. After the three cycles, an additional 3 min of 0.7 V was applied to the gold electrode before the circuit was disconnected. The dichloromethane solution was then decanted immediately. The PVF-coated electrode was rinsed with deionized water and was dried in air for at least 24 h. All the potential values reported in this paper are with respect to saturated calomel electrode unless noted otherwise. This method of deposition has been reported to produce rigid and stable PVF film,[10] which is critical in quartz crystal microbalance (QCM) studies.

Potentiostat and EQCM.— The electrochemical analysis was done with a Bi-Potentiostat (Pine Instrument Co., model AFRDE5). For EQCM, the Bi-Potentiostat was connected to a research QCM (RQCM, Maxtek, Inc.) through the analogue/digital (A/D) switch port. A homemade current integrator, used to record charge, was also connected to the RQCM through the A/D port. The RQCM instrument was connected to the gold plate (the working electrode) through a 470 pF capacitor, preventing interference with the potential-scan circuitry. Typically, the potential swept back and forth linearly for at least four cycles with a scan rate varying from 5 to 200 mV/s and in some cases as low as 2 mV/s. The values of potential, current, charge, quartz resonance frequency, and the damping resistance of the equivalent Butterworth–van Dyke circuit[11] were recorded at a rate of 20 points per s and the data were exported to a PC with Windows 98 operating system for further analysis. A single-compartment cell was used with PVF-coated QCM gold electrode mounted on the side. The QCM gold plate which faced the electrolyte solution was used as the working electrode. Platinum wire was used as the counter electrode. The electrochemical cell contained the 0.1 M control solutions, pure ILs, or 0.1 M IL aqueous solutions.

Control experiment.— The electrochemistry of PVF in 0.1 M $NaClO_4$ has been studied thoroughly; therefore, we chose 0.1 M $NaClO_4$ solution as the control media. Electrochemical and EQCM experiments were performed in 0.1 M $NaClO_4$ before and after tests in the ILs. We also selected another two control salts, TBAP (Bu_4NClO_4) and NaOMs. TBAP is a perchlorate salt with tetrabutylammonium (Bu_4N^+) which is present in some ILs, while NaOMs (sodium methanesulfonate) contains the same anion as the methanesulfonate ILs.

Results and Discussion

[BMIM][BF_4] is currently one of the most studied water-soluble ILs, and in the following report we put the focus on this IL. During the PVF redox cycles, PVF matrix switches between the neutral state and positive-charged state; therefore, doping/undoping of anions is needed to balance the charge change. In order to study the effects of anions, we also need another water-soluble IL which differs from [BMIM][BF_4] in the anion. We selected [PMIM][OMs] rather than [BMIM][OMs] because the latter is a solid at room temperature.

PVF break-in effect in IL.— Break-in effect, also called hysteresis and memory effect, means that several cycles of potential sweeping are needed for a newly made conductive polymer to be fully electroactive.[12] This effect is mainly caused by polymer reconfiguration when solvent molecules and ions are doped or undoped. The number of cycles required for the break-in process depends on the film thickness, the nature and concentration of the supporting electrolyte, the temperature, and the scan rates. In 0.1 M $NaClO_4$, the break-in process for PVF was fast and only the first cycle of the cyclic voltammogram showed a noticeable difference from the following cycles; this difference was only apparent when the potential scan rate was faster than 10 mV/s. In pure ILs such as [BMIM][BF_4] and [PMIM][OMs], the break-in was a much slower process. At a potential scan rate of 200 mV/s, it took several cycles for the current-potential curve to reach steady state (Fig. 1). When a slower scan rate, i.e., 5 or 2 mV/s, was used, the break-in process only showed a different current-potential curve for the first cycle (Fig. 2a). In addition, the first cycle in Fig. 2a is a well-defined one-electron transfer curve, which is different from the first cycle shown in Fig. 1. It was expected that the break-in effect depended on scan rate because the PVF film was given much more time to relax at slower scan rates, and thus only one cycle was needed to reach the steady-state voltammograms.

The reasons why the break-in process was faster in 0.1 M $NaClO_4$ than in pure ILs lie in two facts. First, the PVF-modified electrode was made by anodic oxidation in the dichloromethane solution with 0.1 M TBAP as the electrolyte. The perchlorate ions (ClO_4^-) were doped in the PVF matrix after coating.[9] Thus, the PVF polymer was already reconfigured in its best possible structure for ClO_4^- when it was characterized in 0.1 M $NaClO_4$. The potential scan allowed the ferrocene center on the PVF-coated electrode to be oxidized and reduced. Meanwhile, the anions ClO_4^- had to dope into

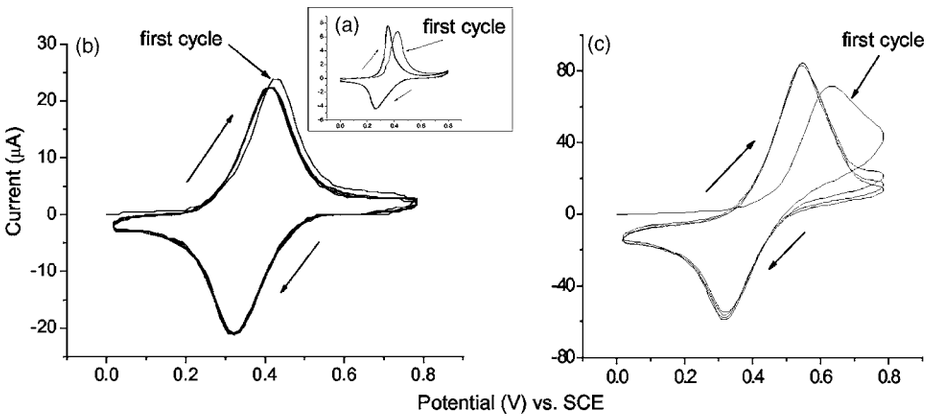

Figure 2. CVs with reduced break-in effect: (a) (inset) Unconditioned newly made PVF-coated electrode at 5 mV/s in [BMIM][BF_4]; (b) 200 mV/s in [BMIM][BF_4]. Electrode conditioned by 40 h soaking; (c) 200 mV/s in [PMIM][OMs]. Electrode conditioned by 40 h soaking.

and undope from the PVF polymer matrix to balance the charge change. The break-in of the anion ClO_4^- into the PVF film was less difficult. Second, considering the viscosity of the ILs, the bulky size of the IL anions, and the interaction between IL anions and IL cations,[13] the slower break-in process for ILs was expected.

We observed two methods to reduce the break-in effects. One was a slow sweep rate, where the polymer matrix had more time to relax according to the potential increase or decrease (Fig. 2a). The other one is conditioning of a newly made PVF-coated electrode in pure ILs ([BMIM][BF_4] or [PMIM][OMs]) at open circuit for 40 h. The cyclic voltammetry showed that only the first cycle was different from the subsequent cycles even when the potential scan rate was as high as 200 mV/s in both ILs. The difference between the first cycle and subsequent cycles was much smaller in [BMIM][BF_4] compared to that in [PMIM][OMs] (Fig. 2b and c). This phenomenon confirmed that various IL-polymer interactions at open circuit facilitated the polymer relaxation process. This finding is highly significant due to the wide diversity of ILs in possible structure and properties. Thus, it is possible to control the solvation/reconfiguration status of the polymer by varying the presoaking duration and/or the nature of ILs.

Water is ubiquitous in the environment. If not stored carefully, the water-soluble IL may absorb moisture from the environment. Water-induced accelerated ion diffusion has been reported.[14] Thus, we studied the effects of water content in IL on the PVF break-in effect. Shown in Fig. 3, a small amount of water moisture increased the rate of ion diffusion and accelerated the PVF relaxation process in pure IL, thus reducing the break-in effect.

The break-in effect reflects the transition of polymer from nonequilibrium condition to dynamic equilibrium condition, where the current-potential voltammogram is constant. Bruckenstein et al. developed a cubic model to explain such transition from nonequilibrium condition to equilibrium condition.[15] The cubic model considered three factors, i.e., coupled electron/ion transfer, solvent transfer, and polymer reconfiguration. Here we describe our simplified model that takes into account two major processes in discussing the break-in effect we observed in the PVF IL system. One is the coupled electron/ion transfer, i.e., the faradaic process. The other is the coupled solvent transfer and polymer reconfiguration, i.e., the nonfaradaic process. In pure ILs, the solvent is actually the ion pair of both anions and cations. This simplification from the cubic model is reasonable because of the following facts. First, the polymer reconfiguration in most cases was the response to the solvent transfer and the coupled electron/ion transfer; therefore, it was not an independent process. Second, reconfiguration was treated as a nonfaradaic process that did not involve charge change; therefore, the cubic model was then simplified to a square model as indicated in Fig. 4.

In the square model, processes of $R_i \rightarrow R_f$ and $O_i \rightarrow O_f$ are nonfaradaic processes and those of $R_i \rightarrow O_i$ and $R_f \rightarrow O_f$ are faradaic processes. Subscripts i and f represent the initial and final states of the PVF before and after nonfaradaic processes. R and O represent the reduced and oxidized forms of PVF. E^0, E_1^0, and E_2^0 are standard reduction potentials for their corresponding faradaic processes. K_1 and K_2 are the equilibrium constants between R and O states. The states of R_f and O_f are stabilized by solvation and polymer reconfiguration; therefore, the nonfaradaic transitions from R_i to R_f and from O_i to O_f are almost irreversible. The reversible transitions from R_f to O_f and from R_i to O_i are driven by the potential and the coupled electron/ion transfer. In our study, we deliberately started potential sweeping from 0.0 V where PVF was at an undoped reduced state. The polymer was not solvated at R_i or O_i states and the pathway $R_i \rightarrow O_i \rightarrow O_f$ was unfavorable because the oxidation from R_i to O_i lacks coupled ion transfer. Consequently, the oxidation of R_i to O_f had to go through an intermediate of R_f state rather than O_i state. By starting the potential sweep from 0.0 V, the O_i state (the

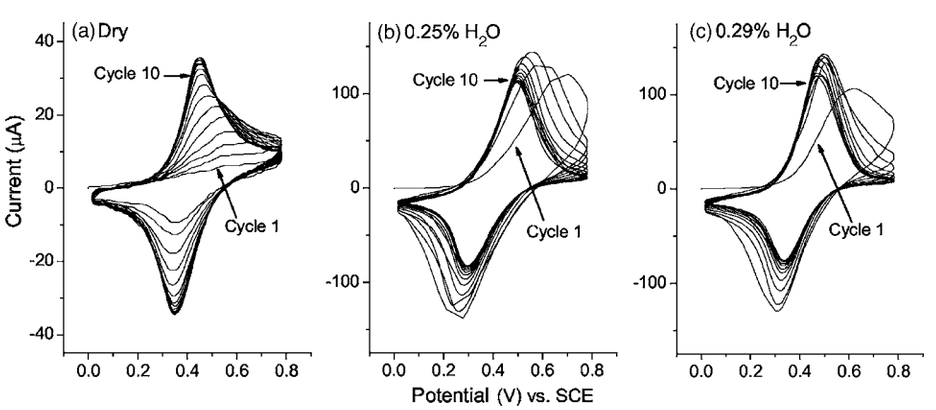

Figure 3. The effect of water content on break-in effect. CVs of newly made PVF films in IL [BMIM][BF_4]: (a) oven-dried pure IL, (b) IL exposed to the atmosphere for 24 h, resulting in a water content of 0.25 wt %, and (c) IL exposed to the atmosphere for 48 h, resulting in a water content of 0.29 wt %.

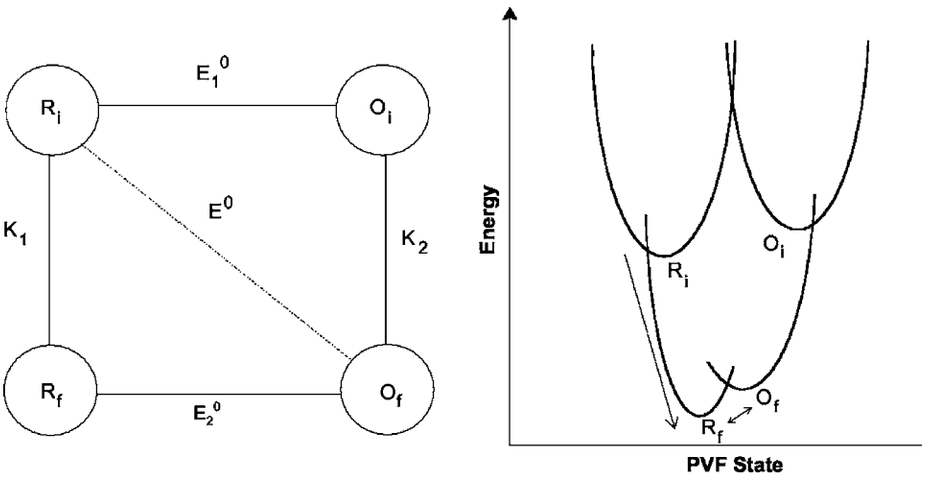

Figure 4. The square model of PVF redox switching and energy diagram. *R* and *O* represent reduced and oxidized forms, respectively. Subscripts of *i* and *f* represent initial and final states, respectively.

unsolvated oxidative initial state of PVF before reconfiguration) did not exist and was only shown for the benefit of discussion. For the pathway $R_i \rightarrow R_f \rightarrow O_f$, only a fraction of R_f was activated by solvation and ion coupling in the first cycle; therefore, the charge change in the first cycle was smaller than in the consequent cycles (Fig. 5). During the first cycle of oxidation, the activated R_f could not go back to the R_i because of the great energy barrier; thus, PVF was populated in the state of activated R_f, resulting in a larger charge change in the following cycle. The amount of charge change increased in each cycle until the nonfaradaic process was completed (Fig. 5).

Figure 1 also shows that the first cycle had no well-defined anodic peak, but it had a well-defined cathodic peak for both pure ILs. This was due to the continuous transition from R_i to R_f as R_f was being transformed to O_f. This led to a constantly increasing population of PVF in the final (*f*) states, making increasing anodic current in the first cycle. On the contrary, the population of PVF was a constant during the cathodic scan because there was no O_i to compensate the consumption of O_f when the O_f was transformed to R_f; as a result, a well-defined cathodic peak current was observed in the first cycle. After about 10 cycles of potential scan, all the PVF stayed in the final (*f*) states, and no more break-in could be observed for later experiments.

Soaking newly made PVF electrode in ILs at open circuit for 40 h reduced the break-in effect, and little difference between the first cycle and subsequent cycles was observed (Fig. 2). When the

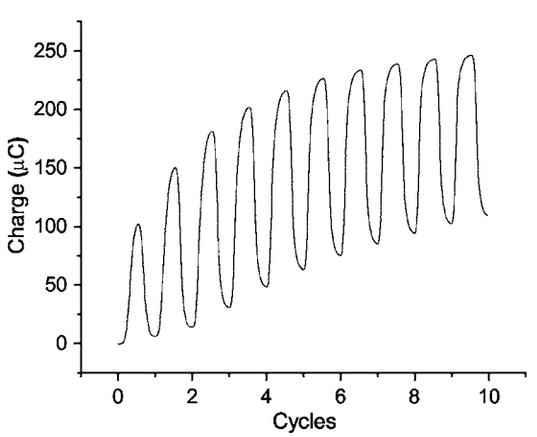

Figure 5. The amount of charge changed with potential sweeping cycles. Newly made PVF-coated electrode in pure [BMIM][BF_4]. Potential scan rate: 200 mV/s.

PVF was in contact with ILs under no potential perturbation, the R_i slowly changed to R_f to reach the equilibrium states that favored R_f via various IL-polymer interactions. As the solvation and polymer reconfiguration lowered the PVF energy greatly, almost all R_i was converted to R_f. No break-in effect was observed in Fig. 2, indicating that the reconfiguration of PVF from R_i to R_f had completed.

Electrochemical characterization of PVF redox switching in ILs and in 0.1 M $NaClO_4$.— For each PVF-coated electrode, cyclic voltammetry was used to characterize PVF properties in 0.1 M $NaClO_4$ before it was studied in IL. Two ILs, [BMIM][BF_4] and [PMIM][OMs], were selected for this study. Our early study showed that the voltammogram of PVF redox switching in [BMIM][BF_4] solution was similar to that in $NaClO_4$, but a significant difference was observed in [PMIM][OMs] solution. The PVF modified electrodes were first conditioned in 0.1 M $NaClO_4$ by electrochemical cycling if they would be used in pure ILs. In this way, the break-in effect was absent.

In Fig. 6, panel A and panel C were of different PVF modified gold electrodes tested in the same 0.1 M $NaClO_4$ solution. The difference shown in these two panels was not a surprise and had been discussed by Bruckenstein et al.[9] In brief, the PVF film thickness and/or density varied for different PVF-coated electrodes even though all experimental conditions were controlled precisely the same. This variation in PVF film caused the variation in the shape of cyclic voltammogram curves.

On the same PVF-coated electrode, the behavior of PVF redox switching in pure [BMIM][BF_4] or in 0.1 M [BMIM][BF_4] solution was similar to that in 0.1 M $NaClO_4$ (Fig. 6). The difference was that the anodic peak potential (E_a) was a little more positive and the cathodic peak potential (E_c) was a little less negative in pure [BMIM][BF_4] than in 0.1 M $NaClO_4$. For example (Fig. 6A and B), at sweep rate of 50 mV/s, E_a in pure [BMIM][BF_4] was 0.02 V more positive than in 0.1 M [BMIM][BF_4], and the E_c was 0.05 V less negative in pure [BMIM][BF_4] than in 0.1 M $NaClO_4$. The same phenomenon was also observed when comparing the 0.1 M [BMIM][BF_4] solution to the 0.1 M $NaClO_4$ solution (Fig. 6C and D). At a sweep rate of 50 mV/s, E_a in 0.1 M [BMIM][BF_4] was 0.06 V more positive than in 0.1 M $NaClO_4$, and the E_c was 0.07 V less negative in 0.1 M [BMIM][BF_4] than in 0.1 M $NaClO_4$. The peak current had a linear relationship with the square root of scan rate, in pure [BMIM][BF_4] or in its 0.1 M solution (Fig. 7), suggesting an apparent diffusion control process. The same linear relationship also held in 0.1 M $NaClO_4$ according to our experiments and previous report.[15]

The similarity of cyclic voltammograms in $NaClO_4$ and in [BMIM][BF_4] may suggest that the doping/undoping mechanism

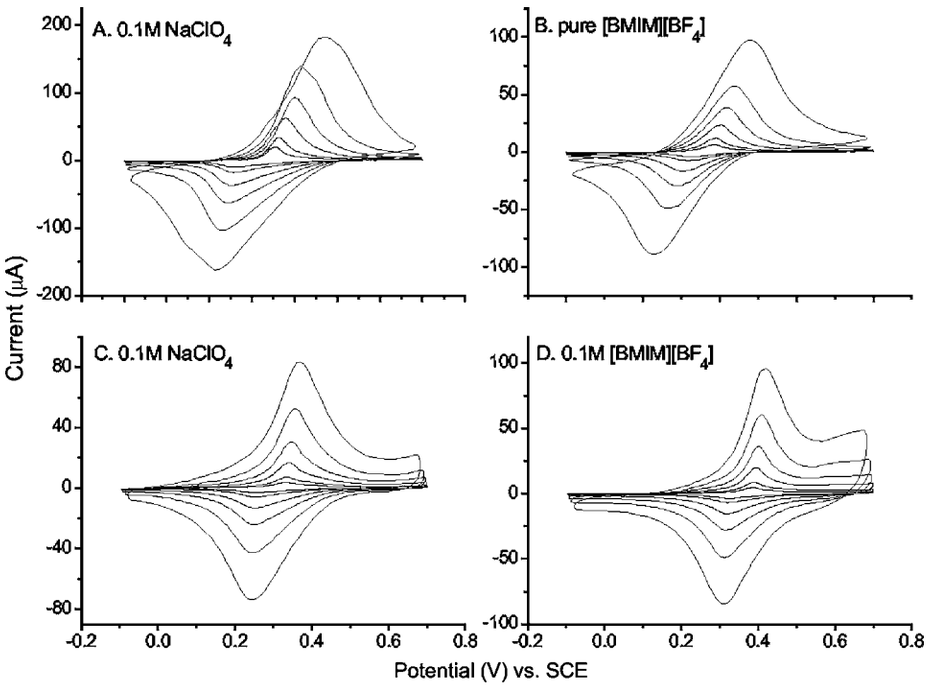

Figure 6. CVs of PVF film in (A and C) 0.1 M $NaClO_4$, (B) pure $[BMIM][BF_4]$, and (D) 0.1 M $[BMIM][BF_4]$. (A) and (B) were of the same PVF film and (C) and (D) were of the same PVF film. The scan rates were 5, 10, 25, 50, 100, and 200 mV/s. Only the third cycle under each scan rate was shown.

was also similar. When PVF was oxidized, anions (ClO_4^- or BF_4^-) were doped into the PVF polymer matrix to balance the excess positive charge. Solvent molecules, if present, might codope with the anions.

The PVF redox behaviors in pure [PMIM][OMs] and in 0.1 M [PMIM][OMs] were different. In pure [PMIM][OMs], the shape of the cyclic voltammogram was similar to that in 0.1 M $NaClO_4$ except that E_a was more positive and E_c was less negative in pure [PMIM][OMs] (Fig. 8A and B). For example, at a sweep rate of 50 mV/s, E_a was 0.08 V more positive in pure [PMIM][OMs] than in 0.1 M $NaClO_4$, and E_c was 0.14 V less negative in pure [PMIM][OMs] than in 0.1 M $NaClO_4$. In 0.1 M [PMIM][OMs] solution, the shape of the cyclic voltammogram was significantly different from that in 0.1 M $NaClO_4$ (Fig. 8C and D). Both the anodic peak and cathodic peak were broader in 0.1 M [PMIM][OMs] than in 0.1 M $NaClO_4$. In addition, the E_a and E_c showed a larger difference from their values in $NaClO_4$. For example, at a sweep rate of 50 mV/s, the E_a in 0.1 M [PMIM][OMs] was about 0.18 V more positive than in 0.1 M $NaClO_4$, and E_c in 0.1 M [PMIM][OMs] was about 0.21 V less negative than in 0.1 M $NaClO_4$. Both anodic and cathodic peak currents in pure [PMIM][OMs] had a linear relationship with the square root of the scan rate. In 0.1 M [PMIM][OMs], the cathodic peak current was linearly proportional to the square root of the scan rate, while the anodic peak current was linearly ($R = 0.996$) related to the scan rate rather than the square root of the scan rate.

Figures 6 and 8 show that the amplitude of the peak current in pure ILs was less than half of that in 0.1 M $NaClO_4$ (panels A and B in both figures). Studies on electron transfer in conductive polymer matrix have indicated that the current is related to the value of apparent diffusion constant, D_{app},[16] which is likely to be affected by the viscosity of the electrolyte.

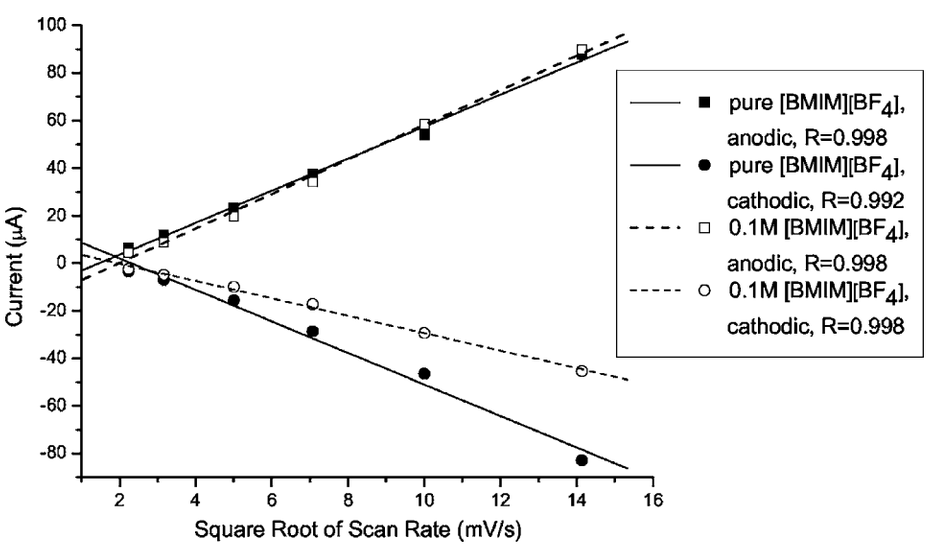

Figure 7. Linear relationship of peak current to the square root of scan rate: (solid points) in pure $[BMIM][BF_4]$ and (empty points) in 0.1 M $[BMIM][BF_4]$.

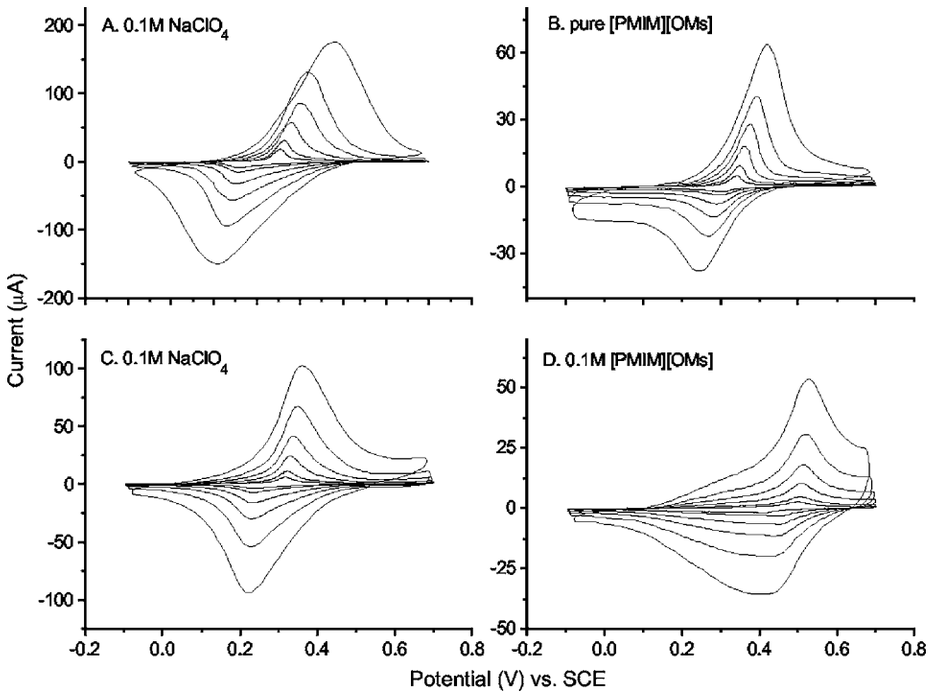

Figure 8. CVs of PVF film in (A and C) 0.1 M $NaClO_4$, (B) pure [PMIM][OMs], and (D) 0.1 M [PMIM][OMs]. (A) and (B) were of the same PVF film and (C) and (D) were of the same PVF film. The scan rates were 5, 10, 25, 50, 100, and 200 mV/s. Only the third cycle under each scan rate was shown.

In 0.1 M [BMIM][BF_4], the peak current was similar to that in 0.1 M $NaClO_4$ (Fig. 6C and D); however, the peak current in 0.1 M [PMIM][OMs] was about half of that in 0.1 M $NaClO_4$ (Fig. 8C and D), indicating that the properties of the cations and anions affect PVF redox mechanisms. EQCMs that could measure mass changes associated with electrochemical processes were further used to characterize the dynamics of PVF undergoing charge-transfer processes in 0.1 M IL solutions in order to obtain additional understanding of the PVF redox mechanism in 0.1 M [BMIM][BF_4] and [PMIM][OMs] solutions.

EQCM.— The EQCM can measure in situ mass changes in the nanogram range. It can demonstrate the existence of adsorbed or doped species on the working electrode and also give much of the information about the change in composition of species on the interface of the working electrode during conductive polymer redox switching processes. In Fig. 9 and 10, the value of electron flow (in moles) is the charge (in coulombs) divided by the Faraday constant. It reflects the number of electrons that moved across the electrode/PVF interface.

The doping/undoping process in 0.1 M [BMIM][BF_4] was simple (Fig. 9a) and was similar to that in 0.1 M $NaClO_4$ as reported by others.[15] When the potential swept to more positive direction, the electron flowed from the PVF matrix to the electrode, with the ferrocene being oxidized to ferrocenium. In order to balance the positive charge in the PVF matrix cause by the oxidation, an equal amount of anions in the [BMIM][BF_4] solution had to dope into the polymer matrix. The slope of 106.6 g/mol (Fig. 9a) resulted from one BF_4^- anion and water molecules, with 86.8 g/mol (the formula weight of BF_4^-) from BF_4^- and the rest of 19.8 g/mol from water. This calculation indicated that about 1.1 molecules of water codoped with each BF_4^- anion. The doping/undoping process in 0.1 M [PMIM][OMs] was more complicated (Fig. 9b). The slope of section b-c was as high as 524.8 g/mol, much larger than the formula weight of the anion OMs^-, 95.1 g/mol. The complicated doping/undoping process shown in 0.1 M [PMIM][OMs] was present in the solution of many ILs, especially those with OMs^- anions. We tested aqueous solutions of six OMs^- ILs, and all

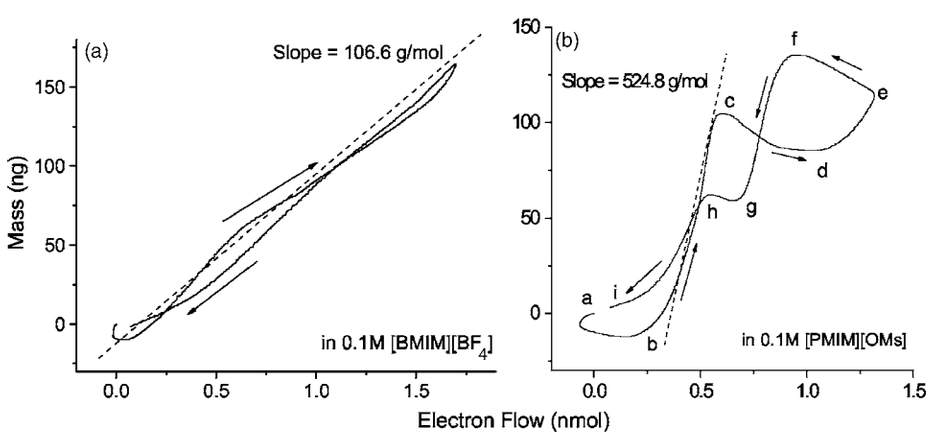

Figure 9. EQCM experiment shows how the mass of PVF matrix changed with the electron flow to the electrode (a) in 0.1 M [BMIM][BF_4] and (b) in 0.1 M [PMIM][OMs]. The break-in processes are completed in third cycles, so only the third cycles of potential sweep are shown. Sweep rate: 5 mV/s. The slope was calculated from the fitted dotted straight line.

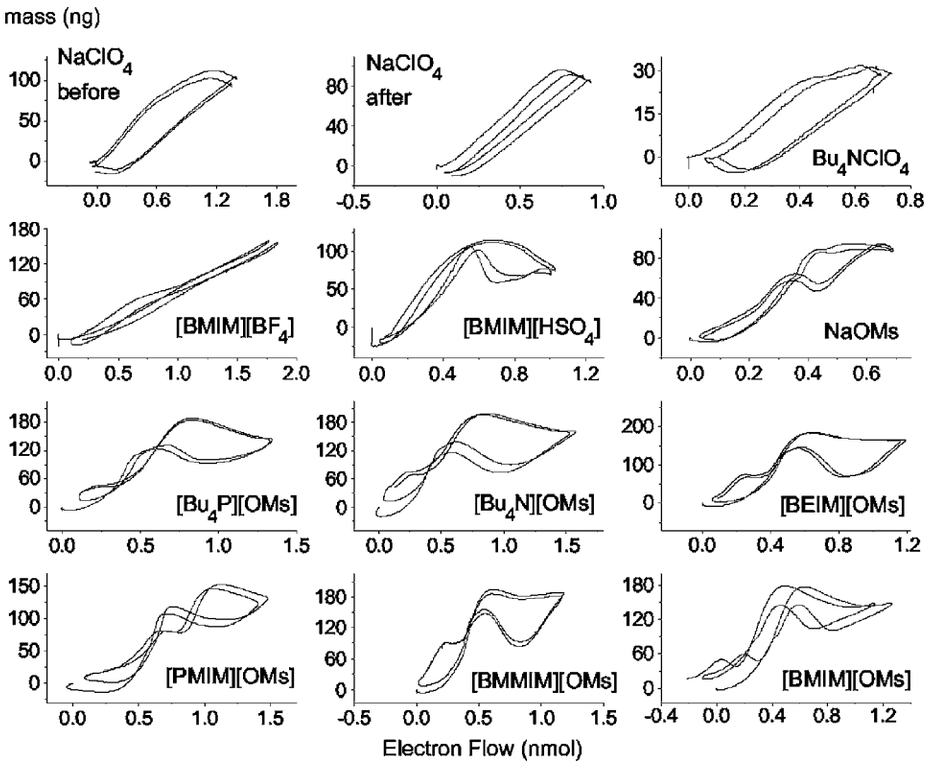

Figure 10. Mass vs electron flow curves for several ILs and controls, all in 0.1 M aqueous solutions. Tests were carried out in $NaClO_4$ before and after the tests in all other chemicals. Two cycles are shown. Sweep rate: 5 mV/s.

of them showed the similar mass-electron flow curves as [PMIM][OMs] (Fig. 10).

The first row in Fig. 10 is of the electrolytes containing ClO_4^- anions. $NaClO_4$ is tested before and after all other electrolytes being studied. Bu_4NClO_4 was used as one of the controls because it was the electrolyte in PVF coating and the cation Bu_4N^+ was a component of some ILs. The second row in Fig. 10 is of two ILs and another control. [BMIM][BF_4] shows a similarity to $NaClO_4$ as discussed in an earlier part of this work. [BMIM][HSO_4] shows some complexity in the doping/undoping process as well as NaOMs. The latter was not an IL and was studied as a control. The last two rows in Fig. 10 are of six ILs with OMs^- anions, which all show complexity similar to [PMIM][OMs]. Although the detailed mechanisms for such complexity are still uncertain, our studies indicate that it is likely related to the anions and probably, at least partially, caused by the ionization equilibrium (or partial ionization) of ILs, which is demonstrated by the following example of the pH value of 0.1 M [BMIM][HSO_4]. The pK_{a2} of H_2SO_4 is 1.99. If [BMIM][HSO_4] had been totally ionized, the sum of [HSO_4^-] and [SO_4^{2-}] would be 0.1 M; therefore, [H^+] would be 0.027 M. However, the measured pH value of 1.95 showed that there was only about 0.011 M protons in the solution, indicating about 41% ionization of the IL. Considering the weak acidity of [BMIM]$^+$ cation and the trace amount of acid in the preparation of IL, the ionization ratio would be even lower.

The model proposed by Anson et al.[17] can be used to describe the details of the doping/undoping process of PVF in IL solutions. In Anson's model, the interior environment of coated polymer was considered to include two regions. One was named the Donnan region, where counterions were electrostatically confined to the vicinity of the polymer chains. The other was the non-Donnan region, with the same constitution as the bulk supporting media, although the concentration might be different. In the case of IL solution, for example, the 0.1 M [PMIM][OMs], the bulk supporting media comprised [PMIM]$^+$ cations, OMs^- anions, [PMIM][OMs] molecules, H_2O molecules, protons (solution pH 2.43), and negligible OH^-.

Shown in Fig. 11, there are several dynamic equilibria in the solid–liquid interfaces. The IL is present in the bulk solution as well as in the non-Donnan region of the PVF polymer matrix. Therefore, the ionization equilibrium of [PMIM][OMs] is present in both bulk solution and the non-Donnan region. This equilibrium is critical to the flux among neutral [PMIM][OMs] molecule, [PMIM]$^+$ cation, and OMs^- anion into the PVF film during the redox switching. The concentration of each species in the bulk solution and the non-

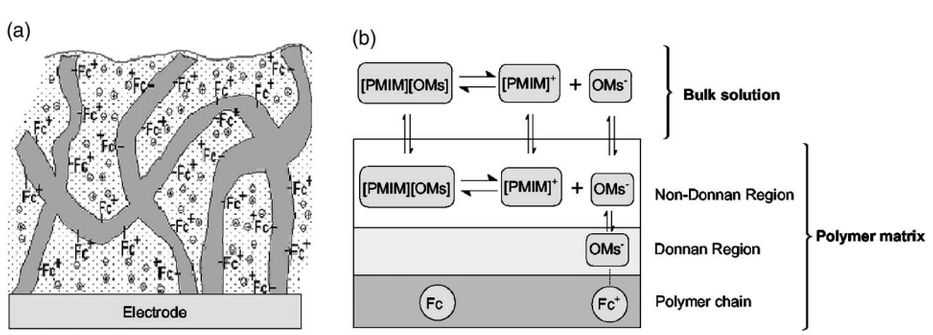

Figure 11. (a) Schematic diagram of oxidized PVF matrix. (b) Schematic diagram of dynamic equilibria between bulk solution and polymer matrix during redox switching of PVF. Fc represents the ferrocene center in PVF.

Donnan region is determined by several partition equilibria. The mass change during PVF redox switching due to the dynamic changes of above equilibria can be monitored by EQCM.

When PVF is oxidized or ferrocene (Fc) is transformed to be ferrocenium (Fc^+), the Donnan region forms with anion OMs^- electrostatically attracted by the Fc^+. This results in a deficiency of OMs^- in the non-Donnan region, and OMs^- has to enter the polymer matrix from the bulk solution to balance the positive charge. This shifts the [PMIM][OMs] ionization equilibrium in both the bulk and non-Donnan domain. Therefore, it is likely that the doping species are composed of neutral [PMIM][OMs] molecules and excessive OMs^- anions. The solvent molecules may also participate in the doping, but we do not consider them in the following discussion. To neglect the effect of the solvent is reasonable, because the molecular weight of a water molecule is smaller when compared to that of [PMIM][OMs] (MW = 220.3 g/mol). In addition, the number of water accompanying each anion in doping is also small;[18] for example, it is 1.1 in the case of $[BMIM][BF_4]$ solution, as mentioned above. When the rate of PVF oxidation is fast, the mass transfer of [PMIM][OMs] and OMs^- cannot balance the fast-generated positive charge in the non-Donnan region. Under this situation, the exclusion of $[PMIM]^+$ from the non-Donnan region to the bulk solution takes place. The model in Fig. 11 is consistent with our data (Fig. 9b). The slope of section b-c in Fig. 9b was caused by entering of [PMIM][OMs] and OMs^-. The slope of 524.8 g/mol suggests that about 2.0 [PMIM][OMs] molecules accompanied each OMs^- anion in doping. Section c-d was due to the exclusion of $[PMIM]^+$ when the entering of [PMIM][OMs]/OMs^- alone could not balance the positive charge generated in the polymer matrix. In section d-e, the mass increased again but with a smaller slope than section b-c. This was a net result of [PMIM][OMs]/OMs^- entering and $[PMIM]^+$ exclusion. Based on this multistep doping mechanism, it is expected that lighter cations generate less mass decrease in the cation exclusion process (section c-d in Fig. 9b). This is confirmed by the case of 0.1 M NaOMs (see Fig. 10), where the exclusion of cation caused little mass decrease.

When the potential sweeps back from the positive end to the negative end (reduction of PVF), Fc^+ is converted to Fc and the negative charge or OMs^- becomes excessive. As a result, either OMs^- needs to leave the polymer matrix or more $[PMIM]^+$ needs to enter the polymer matrix. Our experiment results indicated the latter was the case at the early stage of reduction, as the mass increased in section e-f of Fig. 9b. It is still uncertain what caused such a barrier for OMs^- leaving the polymer matrix, but we assumed one of the reasons was the interaction between OMs^- ion and the ferrocene. The relatively low electronegativity of sulfur (S) caused the higher electron density of oxygen (O) in the OMs^- anion than in ClO_4^-. The higher electron density around oxygen in OMs^- increases the interaction with the empty orbital of Fc in PVF; therefore, the leaving of OMs^- from the Donnan region is restricted. As OMs^- leaving was restricted, $[PMIM]^+$ had to enter the polymer matrix to balance the excessive negative charge generated by PVF reduction.

[BMIM][BF_4] and [PMIM][OMs].— The difference between these two ILs is apparent in the above discussions. First, the break-in effect lasted more cycles for $[BMIM][BF_4]$ than for [PMIM][OMs] (Fig. 1); second, the peak current in $[BMIM][BF_4]$ was larger than in [PMIM][OMs] (Fig. 6 and 8); and third, the doping/undoping in 0.1 M [PMIM][OMs] showed a multistep mechanism (Fig. 9). Although more experimentation is needed to find out the reasons for such differences, the following fact might play a role to some degree. The spherical shape of BF^- was similar to ClO_4^-, making the IL anion penetrate to a deeper inner layer of PVF matrix. On the contrary, OMs^- ($CH_3SO_3^-$) could only activate the ferrocene close to the PVF/liquid interface. In other words, the amount of fully activated ferrocene in $[BMIM][BF_4]$ was larger than that in [PMIM][OMs]. The result was that the PVF polymer could be fully electroactivated faster in [PMIM][OMs] than in $[BMIM][BF_4]$. Compared to the spherical shape, the "rod-shaped" OMs^- caused anisotropy in cation/anion interaction, resulting in lower conductivity for the [PMIM][OMs].[19] The smaller peak current in [PMIM][OMs] than in $[BMIM][BF_4]$ was thus expected. The anisotropy caused by the nonsphere shape of anions also made ionization difficult. That is why we observed multistep doping/undoping in 0.1 M [PMIM][OMs] but not in 0.1 M $[BMIM][BF_4]$. In fact, the multistep doping/undoping is a general phenomenon for methanesulfonate IL solutions (Fig. 10).

Conclusions

Our study shows that the ionization of ILs and the counterion migration play an important role in the redox switching of PVF coated electrode in IL electrolyte. The mechanisms of PVF redox switching in pure $[BMIM][BF_4]$ and 0.1 M $[BMIM][BF_4]$ solutions are similar to those in 0.1 M aqueous $NaClO_4$, likely due to the similarity of the anions. However, in methanesulfonate ILs, not only the anions but also the molecules of IL interact with the PVF matrix, suggesting the existence of the strong IL-polymer interaction. The cations were later removed from the PVF matrix to balance the excessive positive charge during oxidation. The strong IL-polymer interaction in certain ILs (e.g., methanesulfonate ILs) may change the polymer sublattice structure. Thus, ILs tremendous diversity in structural and chemical properties and their distinctive properties offer us an excellent opportunity to explore IL-polymer interactions to dynamically control the polymer relaxation process and their redox switching mechanism for various applications such as fuel cells, electrical wire, semiconductor devices, energy storage in batteries, and environmental sensors of toxic species.

Acknowledgment

The research was supported by Oakland University Research Excellence Fund and faculty start-up funds. The authors thank Dr. Rex Ren of IL-TECH, Inc. for providing many of the ionic liquids. Yijun Tang also thanks the Oakland University Provost's Graduate Student Research Award and the Oakland University Research Excellence Fund.

Oakland University assisted in meeting the publication costs of this article.

References

1. A. L. Nguyen and J. H. T. Luong, *Appl. Biochem. Biotechnol.*, **43**, 117 (1993); *Molecular Design of Electrode Surface*, R. W. Murray, Editor, Vol. xxii, John Wiley and Sons, New York (1992); S. Dong and G. Che, *J. Electroanal. Chem. Interfacial Electrochem.*, **309**, 103 (1991); X. B. Wang, J. M. Bonnett, R. Pethig, P. K. Baker, O. L. Parri, and A. E. Underhill, *J. Mol. Electron.*, **7**, 167 (1991); T. Kawai, C. Iwakura, and H. Yoneyama, *Electrochim. Acta*, **34**, 1357 (1989); A. R. Hillman, in *Electrochemical Technology of Polymers*, R. Linford, Editor, pp. 241–291, Elsevier Applied Science Publishers, London (1987); R. M. Kannuck, J. M. Bellama, E. A. Blubaugh, and R. A. Durst, *Anal. Chem.*, **59**, 1473 (1987).
2. G. Inzelt, in *Electroanalytical Chemistry: A Series of Advances*, Vol. 18, A. J. Bard, Editor, p. 146, CRC Press, Boca Raton, FL (1994).
3. S. Bruckenstein and A. R. Hillman, *J. Phys. Chem.*, **95**, 10748 (1991); P. T. Varineau and D. A. Buttry, *J. Phys. Chem.*, **91**, 1292 (1987); P. Daum and R. W. Murray, *J. Phys. Chem.*, **85**, 389 (1981).
4. A. Fernicola, B. Scrosati, and H. Ohno, *Ionics*, **12**, 95 (2006); T. E. Sutto, M. Ollinger, H. S. Kim, C. B. Arnold, and A. Pique, *Electrochem. Solid-State Lett.*, **9**, A69 (2006); J. N. Barisci, G. G. Wallace, D. R. MacFarlane, and R. H. Baughman, *Electrochem. Commun.*, **6**, 22 (2004); S. T. Handy, *Chem.-Eur. J.*, **9**, 2938 (2003); J. Ding, D. Z. Zhou, G. Spinks, G. Wallace, S. Forsyth, M. Forsyth, and D. MacFarlane, *Chem. Mater.*, **15**, 2392 (2003); M. P. Jensen, J. Neuefeind, J. V. Beitz, S. Skanthakumar, and L. Soderholm, *J. Am. Chem. Soc.*, **125**, 15466 (2003); C. Yang, Q. J. Sun, J. Qiao, and Y. F. Li, *J. Phys. Chem. B*, **107**, 12981 (2003); P. Wang, S. M. Zakeeruddin, J. E. Moser, and M. Graetzel, *J. Phys. Chem. B*, **107**, 13280 (2003); A. B. McEwen, H. L. Ngo, K. LeCompte, and J. L. Goldman, *J. Electrochem. Soc.*, **146**, 1687 (1999).
5. C. Decastro, E. Sauvage, M. H. Valkenberg, and W. F. Hölderich, *J. Catal.*, **196**, 86 (2000); P. G. Pickup and R. A. Osteryoung, *J. Electrochem. Soc.*, **130**, 1965 (1983).
6. M. C. Buzzeo, R. G. Evans, and R. G. Compton, *ChemPhysChem*, **5**, 1106 (2004).
7. D. B. Zhao, M. Wu, Y. Kou, and E. Z. Min, *Catal. Today*, **74**, 157 (2002); H. Olivier-Bourbigou and L. Magna, *J. Mol. Catal. A: Chem.*, **182–183**, 419 (2002).
8. J. Bacskai and G. Inzelt, *J. Electroanal. Chem. Interfacial Electrochem.*, **310**, 379 (1991).

9. S. Bruckenstein, E. Pater, and A. R. Hillman, *Anal. Chem.*, **72**, 1598 (2000).
10. A. R. Hillman, D. C. Loveday, and S. Bruckenstein, *Langmuir*, **7**, 191 (1991).
11. D. A. Buttry and M. D. Ward, *Chem. Rev. (Washington, D.C.)*, **92**, 1355 (1992).
12. G. Inzelt, *Chem. Biochem. Eng. Q.*, **21**, 1 (2007).
13. W. Yoshizawa, A. Naritz, and H. Ohno, *Aust. J. Chem.*, **57**, 139 (2004).
14. U. Schröder, J. D. Wadhawan, R. G. Compton, F. Marken, P. A. Z. Suarez, C. S. Sonsorti, R. F. de Souze, and J. Dupont, *New J. Chem.*, **24**, 1009 (2000).
15. S. Bruckenstein, P. Krtil, and A. R. Hillman, *J. Phys. Chem. B*, **102**, 4994 (1998).
16. M. Majda, *Molecular Design of Electrode Surface*, Vol. xxii, R. W. Murray, Editor, Chap. 4, John Wiley and Sons, New York (1992).
17. F. C. Anson, J.-M. Saveant, and K. Shigehara, *J. Am. Chem. Soc.*, **105**, 1096 (1983).
18. A. R. Hillman, D. C. Loveday, and S. Bruckenstein, *J. Electroanal. Chem. Interfacial Electrochem.*, **274**, 157 (1989).
19. S. Tsuzuki, H. Tokuda, K. Hayamizu, and M. Watanabe, *J. Phys. Chem. B*, **109**, 16474 (2005).